

On different models describing the equilibrium shape of erythrocyte

G. S. Valchev*, V. M. Vassilev, P. A. Djondjorov

Institute of Mechanics, Bulgarian Academy of Sciences, Acad. Georgy Bonchev Str., Bl. 4, 1113 Sofia, Bulgaria

Red blood cells (erythrocytes) fall to one of the most important families of cells in all vertebrate organisms. The study of the equilibrium shapes of this kind of cells is of particular importance for the understanding of their physical, chemical and mechanical properties. In the present work, several well-known and widely acknowledged models describing the equilibrium shapes of the red blood cells are analysed. For each of the regarded models we make a comparison between the shapes of the meridional contours predicted by it and the known experimental data. The obtained results can be used to choose a suitable model for the analytical study of the interactions between individual erythrocytes or between them and the walls of blood vessels, for the diagnosis of diseases associated with a change of the equilibrium shape of the cells or for the experimental study of the red blood cells by light scattering methods.

Key words: Red blood cells, Erythrocytes, Equilibrium shapes, Cassinian ovals

1. INTRODUCTION

The red blood cells (RBCs) or erythrocytes are the most common type of blood cell in all vertebrate organisms. They are responsible for the delivery of oxygen (O_2) from the respiration organs (lungs, gills, skin) to the body tissues and the return transport of carbon dioxide (CO_2) from the tissues via the blood flow through the circulatory system. This type of cells have specific biophysical properties for responding to a change in the local chemical and mechanical environment. Any deviation from these regular biophysical properties (regular shapes, for instance) impair the normal functions of RBCs in the human body and is a sensitive marker for various blood disorders and diseases, e.g., malaria and sickle cell anemia. For this reason, the development of relevant techniques for obtaining the biophysical characteristics of the RBCs have been of paramount significance in medical diagnostics [1].

Normal mature RBCs are shaped as biconcave oblate discs, which deform with pressure and physiological conditions in blood. This unique shape determines a large surface-area-to-volume ratio. The typical model geometry of a RBC is assumed to be axially symmetric, with the meridional cross-section characterised by the following morphological parameters [2]: the diameter – D , the dimple (minimal) thickness – τ_{\min} , the maximum thickness – τ_{\max} , and the diameter of a circle that determines the location of the maximum thickness – d .

Several well-known and widely acknowledged

models describing the equilibrium (biconcave) shape of the RBCs are analysed in the present work. For each model we give the relationship between the aforementioned morphological parameters and those used in the particular model. Analytic expressions for the surface area, volume and sphericity index are also obtained. Starting with the lowest degree polynomial approximation suggested by Beck [3], and ending with the highest one proposed by Evans and Fung [4], we compare the meridional contours predicted by each of these models with a set of experimental data (for concrete values of the morphological parameters characterising those contours see Table 1).

Table 1. Values of the morphological parameters and albumin tonicities of RBC solutions, taken from Ref. [4] (Cell 1 and Cell 2) and Ref. [5] (Cell 3 and Cell 4). The red blood cells in cases "Cell 1" and "Cell 2" were obtained from a 30-year-old male, separated into four samples, centrifuged at 4000 rpm for 20 min, and the plasma and white cell layer were removed. The packed RBCs were then diluted by a factor of ten with Eagle-albumin solution, centrifuged again and the Eagle-albumin solution removed. In cases "Cell 3" and "Cell 4" the erythrocytes were obtained, by finger-prick, from seven apparently healthy subjects (male and female), and drawn into micro-haematocrit capillaries coated with sodium heparin. About 0.05 ml of the blood was added to 5 ml of an isotonic THAM–HCl–buffered Ringer solution (10 mM THAM, pH 7.4 ± 0.02) with (in case "Cell 4") and without (in case "Cell 3") albumin.

	D [μm]	d [μm]	τ_{\max} [μm]	τ_{\min} [μm]	albumin tonicity [mOsmol]
Cell 1	7.59	4.68	3.26	2.08	217
Cell 2	7.82	5.52	2.52	0.81	300
Cell 3	8.04	5.30	2.62	1.54	0
Cell 4	7.64	4.55	2.86	1.45	310

* To whom all correspondence should be sent:
gvalchev@imbm.bas.bg

In our opinion, the results presented here would be helpful for one to choose a suitable model for the specific purposes of its usage, e.g., for analytical study of the interactions between individual erythrocytes or between them and the walls of blood vessels, for the diagnosis of diseases associated with a change of the equilibrium shape of the cells, and for the experimental study of the RBCs by light scattering methods.

The article is arranged as follows: in Section 2 we introduce the Beck model. Sections 3.1 and 3.2 are focused on models based on Cassinian ovals. In Sections 3.3 and 3.4 we comment a model proposed by Kuchel and Fackerell, later on modified by Yurkin. The last two models that we analyse are those of Fung and Tong in Section 4.1 and Evans and Fung in Section 4.2. The article ends with a discussion and concluding remarks – Section 5.

2. QUADRATIC POLYNOMIAL APPROXIMATION – BECK'S MODEL

The mathematical representation of the meridional cross-section of a RBC used by Beck [3] is that of the arcs of two circles, one being the cross-section of a torus at the periphery of the cell centred on the x -axis, and another one, which is centred on the z -axis (the axis of revolution), representing the dimple region. These arcs are constrained to be continuous with equal first derivatives at a specified value x_0 . The equation of the resulting curve is obtained by writing separate expressions for the two arcs over their respective intervals

$$z = \begin{cases} C_{0B} + \frac{\tau_{\min}}{2} - \sqrt{C_{0B}^2 - x^2}, & 0 \leq x \leq x_0 \\ \sqrt{\frac{D}{4}(2\tau_{\max} - D) + (D - \tau_{\max})x - x^2}, & x_0 < x < \frac{D}{2} \end{cases} \quad (1)$$

where

$$C_{0B} = \frac{D(D - 2\tau_{\max}) + \tau_{\min}^2}{4(\tau_{\max} - \tau_{\min})} \quad \text{and} \quad x_0 = \frac{(D - \tau_{\max})C_{0B}}{2C_{0B} + \tau_{\max}}. \quad (2)$$

Once the approximated meridional cross-section of a RBC is given in an explicit analytic form, one can easily derive expressions for the surface area A , volume V and sphericity index Ψ of these cells. Using simple mathematical techniques (see p. 364 and p. 572 in [6]) one obtains

$$A = 4\pi \int_0^{D/2} x \sqrt{1 + \left(\frac{dz}{dx}\right)^2} dx, \quad V = 4\pi \int_0^{D/2} x z dx, \quad \Psi = \frac{\pi^{1/3}(6V)^{2/3}}{A}. \quad (3)$$

Within this model, Beck obtained the following analytical expressions for the above mentioned quantities

$$A_B = 4\pi \left\{ C_{0B} \left(C_{0B} - \sqrt{C_{0B}^2 - x_0^2} \right) + \frac{\tau_{\max}}{2} \left[C_{1B} + \frac{D - \tau_{\max}}{2} \left(\frac{\pi}{2} - \arcsin C_{2B} \right) \right] \right\}, \quad (4a)$$

where

$$C_{1B} = \sqrt{\frac{D}{4}(2\tau_{\max} - D) + (D - \tau_{\max})x_0 - x_0^2} \quad \text{and} \\ C_{2B} = \frac{2x_0 - D + \tau_{\max}}{\tau_{\max}};$$

$$V_B = \frac{4}{3}\pi \left\{ \frac{3}{4}(2C_{0B} + \tau_{\min})x_0^2 + \left[(C_{0B}^2 - x_0^2)^{3/2} - C_{0B}^3 + C_{1B}^3 \right] \right. \\ \left. + \frac{3\tau_{\max}(D - \tau_{\max})}{8} \left[\frac{\tau_{\max}}{2} \left(\frac{\pi}{2} - \arcsin C_{2B} \right) - C_{1B}C_{2B} \right] \right\}; \quad (4b)$$

$$\Psi_B = \frac{\pi^{1/3}(6V_B)^{2/3}}{A_B}. \quad (4c)$$

A comparison between the meridional contours of RBCs predicted by Beck's model and the experimentally obtained data can be seen in Figures 1 and 2.

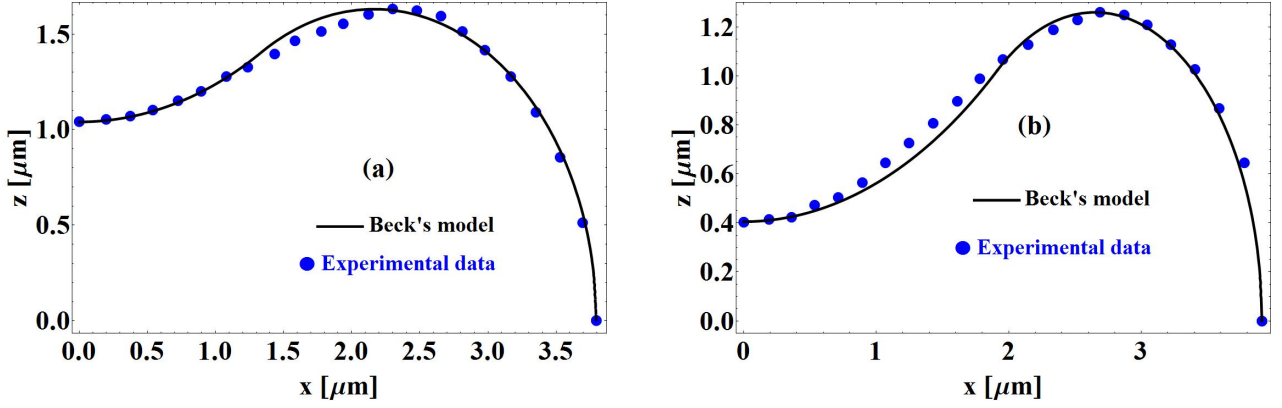


Fig. 1. Meridional contours of RBCs obtained via Beck's model (the black thick curves) in comparison to experimentally obtained ones [(Cell 1 in (a)) and (Cell 2 in (b)) (•)] of normal red blood cells taken from [4] (see also [7]). Only one quadrant of the contour is shown. For the values of the model parameters one has: (a) $C_{0B} = 2.64 \mu\text{m}$ and $x_0 = 1.34 \mu\text{m}$; (b) $C_{0B} = 3.27 \mu\text{m}$ and $x_0 = 1.91 \mu\text{m}$.

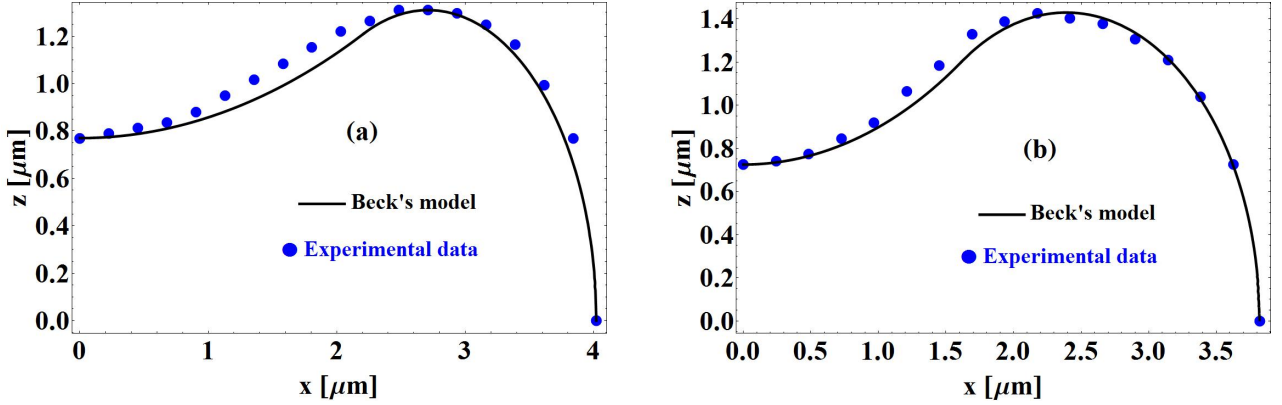


Fig. 2. Meridional contours of RBCs obtained via Beck's model (the black thick curves) in comparison to experimentally obtained ones [Cell 3 in (a)) and (Cell 4 in (b)) (•)] of normal red blood cells taken from [5]. Only one quadrant of the contour is shown. For the values of the model parameters one has: (a) $C_{0B} = 5.76 \mu\text{m}$, $x_0 = 2.21 \mu\text{m}$; (b) $C_{0B} = 2.97 \mu\text{m}$, $x_0 = 1.61 \mu\text{m}$.

3. BIQUADRATIC POLYNOMIAL APPROXIMATIONS

3.1. Model based on single loop Cassinian ovals

Modelling the equilibrium biconcave shape of RBCs via Cassinian ovals is the simplest and probably the most widely used technique [8–21]. Within the framework of this description the meridional cross-section of the considered cells in the (x, z) -plane is given by the equation

$$(a^2 + x^2 + z^2)^2 - 4a^2x^2 = c^4, \quad (5)$$

where the parameters a and c are such that for a point on that curve, the product of its distances from two fixed points (the foci) a distance $2a$ apart is a constant

c^2 . The shape of a curve given by Eq. (5) depends, up to similarity, on the ratio $\varepsilon = c/a$. When $\varepsilon > 1$ (or $c > a$), the curve is a single, connected loop enclosing both foci, while when $\varepsilon < 1$ (or $c < a$), the curve consists of two disconnected loops each of which containing a focus. In the limiting case $\varepsilon = 1$, the curve is the lemniscate of Bernoulli.

In order that the considered description of the equilibrium shape has physical meaning one must relate the two parameters a and c with the morphological ones. For this relationship one finds

$$\begin{aligned} \tau_{\min} &= 2\sqrt{c^2 - a^2}, & \tau_{\max} &= \frac{c^2}{a}, \\ D &= 2\sqrt{c^2 + a^2} \end{aligned} \quad (6)$$

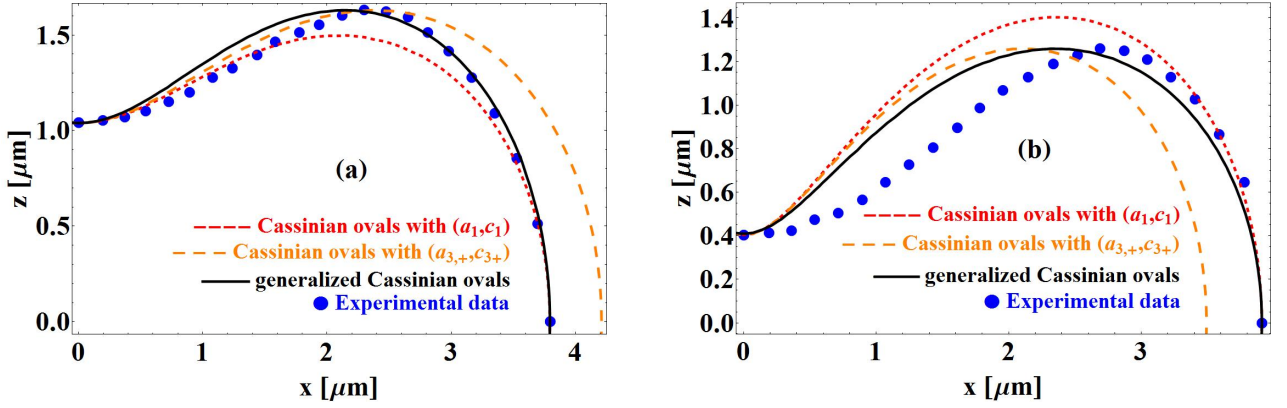


Fig. 3. Contours of RBCs modeled via Cassinian [(-----) and (-----)] and generalized Cassinian ovals (——) in comparison to an experimentally obtained contours [Cell 1 in (a)] and [Cell 2 in (b)] (•) of normal red blood cells taken from [4]. The red short-dashed curve (-----) corresponds to the set of parameters (a_1, c_1) , while the orange long-dashed one (-----) to $(a_{3,+}, c_{3,+})$. In case (a) for the values of the parameters of the Cassinian ovals one has: $a_1 = 2.58 \mu\text{m}$, $c_1 = 2.78 \mu\text{m}$ and $a_{3,+} = 2.89 \mu\text{m}$, $c_{3,+} = 3.07 \mu\text{m}$, while for those of the generalized Cassinian ovals the result is: $a_g = 2.60 \mu\text{m}$, $b = 1.11$ and $c_g = 2.76 \mu\text{m}$. In case (b) these values are as follows: $a_1 = 2.75 \mu\text{m}$, $c_1 = 2.78 \mu\text{m}$; $a_{3,+} = 2.45 \mu\text{m}$, $c_{3,+} = 2.49 \mu\text{m}$; $a_g = 2.75 \mu\text{m}$, $b = 0.89$ and $c_g = 2.78 \mu\text{m}$.

From Eqs. (6) we have

$$a_1 = \frac{\sqrt{D^2 - \tau_{\min}^2}}{2\sqrt{2}}, \quad c_1 = \frac{\sqrt{D^2 + \tau_{\min}^2}}{2\sqrt{2}}; \quad (7a)$$

$$a_2 = \frac{\sqrt{D^2 + \tau_{\max}^2} - \tau_{\max}}{2}, \quad (7b)$$

$$c_2 = \frac{\sqrt{\tau_{\max} \sqrt{D^2 + \tau_{\max}^2} - \tau_{\max}^2}}{\sqrt{2}};$$

$$a_{3,\pm} = \frac{1}{2} \left(\tau_{\max} \pm \sqrt{\tau_{\max}^2 - \tau_{\min}^2} \right), \quad (7c)$$

$$c_{3,\pm} = \frac{1}{\sqrt{2}} \sqrt{\tau_{\max}^2 \pm \tau_{\max} \sqrt{\tau_{\max}^2 - \tau_{\min}^2}}.$$

Comparing each pair of parameters and taking into account the condition for closeness of the ovals ($c > a$), one concludes that only the curves characterized by (a_1, c_1) [see Eq. (7a)] and $(a_{3,+}, c_{3,+})$ [see Eq. (7c)] resemble the meridional cross-section of a RBC (see Figures 3 and 4).

Substituting Eq. (5) in Eq. (3) we find that within the model based on Cassinian ovals one has

$$A_C = 4\pi c^2 \mathcal{A}_C(\varepsilon), \quad (8a)$$

where

$$\mathcal{A}_C(\varepsilon) = \sqrt{\varepsilon^2 - 1} \left\{ E\left[\frac{\pi}{2}, k(\varepsilon)\right] - E[\varphi(\varepsilon), k(\varepsilon)] \right. \\ \left. + F[\varphi(\varepsilon), k(\varepsilon)] - F\left[\frac{\pi}{2}, k(\varepsilon)\right] \right\},$$

$$k(\varepsilon) = \sqrt{\frac{1 + \varepsilon^2}{1 - \varepsilon^2}},$$

$$\varphi(\varepsilon) = \arcsin\left(\sqrt{\frac{\varepsilon^2 - 1}{\varepsilon^2 + 1}}\right);$$

$$V_C = \frac{4}{3}\pi c^3 \mathcal{V}_C(\varepsilon), \quad (8b)$$

where

$$\mathcal{V}_C(\varepsilon) = \frac{1}{4\varepsilon^3} \left\{ (2 + \varepsilon^2) \sqrt{\varepsilon^2 - 1} \right. \\ \left. + 3\varepsilon^4 \left[\frac{\pi}{4} - \arctan\left(\frac{\varepsilon^2 - 2}{\varepsilon^2 + 2\sqrt{\varepsilon^2 - 1}}\right) \right] \right\};$$

$$\Psi_C(\varepsilon) = \frac{\mathcal{V}_C^{2/3}(\varepsilon)}{\mathcal{A}_C(\varepsilon)}. \quad (8c)$$

Note that the relationship between the morphological parameters and those of the Cassinian ovals is *not unique* [see Eqs. (7)] since the dimensionless parameter ε can be either $\varepsilon_1 \equiv c_1/a_1$ or $\varepsilon_{3,+} \equiv c_{3,+}/a_{3,+}$. In Eq. (8a) $F[\varphi(\varepsilon), k(\varepsilon)]$ and $E[\varphi(\varepsilon), k(\varepsilon)]$ denote the first, and respectively the second kind of incomplete elliptic integrals.

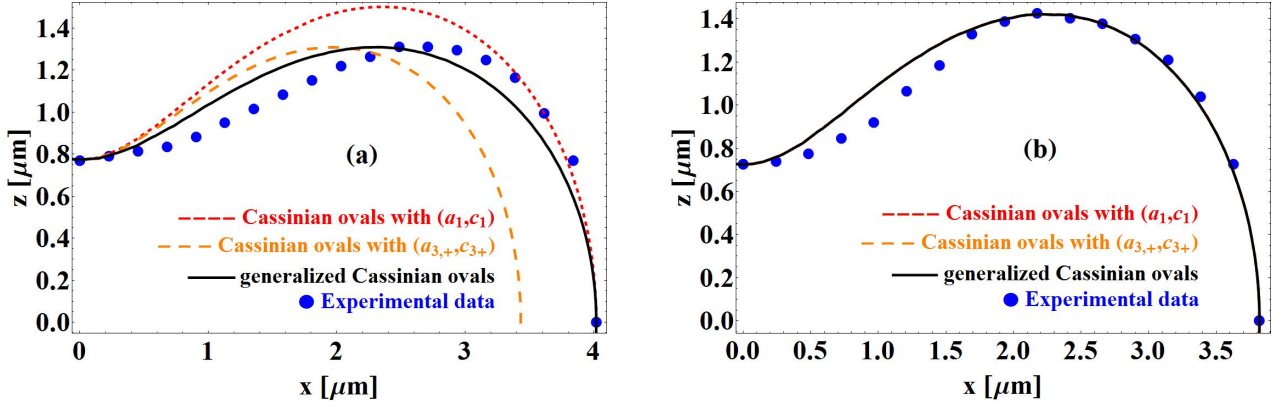


Fig. 4. Contours of RBCs modeled via Cassinian [(-----) and (---)] and generalized Cassinian ovals (—) in comparison to experimentally obtained contours [Cell 3 in (a)] and [Cell 4 in (b)] (•) of normal red blood cells taken from [5]. The short-dashed curve (-----) corresponds to the set of parameters (a_1, c_1) , while the orange long-dashed one (---) to $(a_{3,+}, c_{3,+})$. For the values of the parameters of the Cassinian and generalized Cassinian ovals one finds that: (a) $a_1 = 2.79 \mu\text{m}$, $c_1 = 2.84 \mu\text{m}$; $a_{3,+} = 2.65 \mu\text{m}$, $c_{3,+} = 2.75 \mu\text{m}$; $a_g = 2.77 \mu\text{m}$, $b = 0.86$ and $c_g = 2.91 \mu\text{m}$ and (b) $a_1 = a_{3,+} = a_g = 2.65 \mu\text{m}$, $c_1 = c_{3,+} = c_g = 2.75 \mu\text{m}$ and $b = 1.00$.

3.2. Model based on single loop generalized Cassinian ovals

In order to avoid the lack of uniqueness in the relationship between the morphological parameters and those of the Cassinian ovals, one could introduce an additional degree of freedom (parameter) in Eq. (5) [22–25]. The equation which determines such a generalized Cassinian oval reads

$$(a_g^2 + x^2 + b^{-2}z^2)^2 - 4a_g^2x^2 = c_g^4, \quad (9)$$

where now one has

$$\begin{aligned} \tau_{\min} &= 2b\sqrt{c_g^2 - a_g^2}, \\ \tau_{\max} &= b\frac{c_g^2}{a_g}, \\ D &= 2\sqrt{c_g^2 + a_g^2}. \end{aligned} \quad (10)$$

Hence we find that

$$\begin{aligned} a_g &= \frac{\sqrt{b^2D^2 - \tau_{\max}^2} - \tau_{\max}}{2b}, \\ b &= \frac{\sqrt{4\tau_{\max}\sqrt{\tau_{\max}^2 - \tau_{\min}^2} + 4\tau_{\max}^2 - \tau_{\min}^2}}{D}, \\ c_g &= \frac{\sqrt{\tau_{\max}\sqrt{b^2D^2 + \tau_{\max}^2} - \tau_{\max}^2}}{\sqrt{2}b}. \end{aligned} \quad (11)$$

For the surface area, volume and sphericity index within this model one has

$$\begin{aligned} A_{gC} &= 4\pi b^2 c_g^2 \mathcal{S}_C(\varepsilon), \\ V_{gC} &= \frac{4}{3}\pi b c_g^3 \mathcal{V}_C(\varepsilon), \\ \Psi_{gC} &= b^{-4/3} \frac{\mathcal{V}_C^{2/3}(\varepsilon)}{\mathcal{A}_C(\varepsilon)}, \end{aligned} \quad (12)$$

where the dimensionless functions $\mathcal{S}_C(\varepsilon)$ and $\mathcal{V}_C(\varepsilon)$ are defined in Eqs. (8), and $\varepsilon \equiv c_g/a_g$.

3.3. Kuchel–Fackerell’s model

Within the model suggested by Kuchel and Fackerell [26] the equation for the meridional cross-section of a RBC has the form

$$(x^2 + z^2)^2 + C_{0KF}x^2 + C_{1KF}z^2 + C_{2KF} = 0, \quad (13)$$

where the parameters of the model C_{iKF} , $i = 0, 1, 2$ are related to the morphological ones in the following way

$$\begin{aligned} C_{0KF} &= -\frac{D^2}{2} + \frac{\tau_{\max}^2}{2} \left(\frac{D^2}{\tau_{\min}^2} - 1 \right) \\ &\quad - \frac{\tau_{\max}^2}{2} \left(\frac{D^2}{\tau_{\min}^2} - 1 \right) \sqrt{1 - \frac{\tau_{\min}^2}{\tau_{\max}^2}}, \end{aligned} \quad (14a)$$

$$C_{1KF} = \frac{D^2}{\tau_{\min}^2} C_{0KF} + \frac{\tau_{\max}^2}{4} \left(\frac{D^4}{\tau_{\min}^4} - 1 \right), \quad (14b)$$

$$C_{2KF} = -\frac{D^2}{4} C_{0KF} - \frac{D^4}{16}.$$

The corresponding surface area, volume and sphericity index within the model are

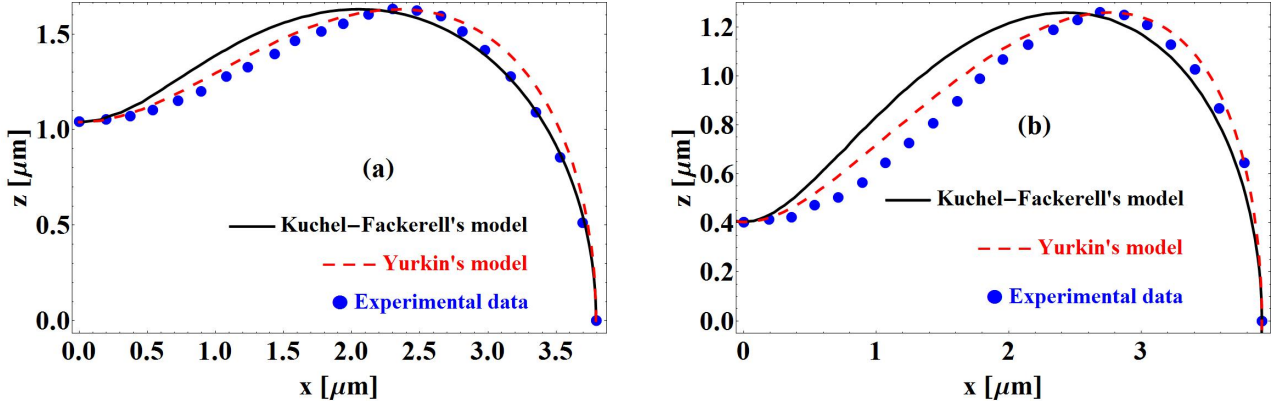


Fig. 5. Contours of RBCs modeled via Kuchel–Fackerell’s model (—) and Yurkin’s one (---) in comparison to experimentally obtained contours [Cell 1 in (a)] and [Cell 2 in (b)] (•) of normal red blood cells taken from [4]. For the parameters of the considered models in case (a) one has: $C_{0KF} = -13.75 \mu\text{m}^2$, $C_{1KF} = 7.56 \mu\text{m}^2$, $C_{2KF} = 9.35 \mu\text{m}^4$; $C_{0Y} = 0.42$, $C_{1Y} = -13.17 \mu\text{m}^2$, $C_{2Y} = 15.29 \mu\text{m}^2$, $C_{3Y} = -17.71 \mu\text{m}^4$, while in case (b) their values are as follows: $C_{0KF} = -15.04 \mu\text{m}^2$, $C_{1KF} = 22.97 \mu\text{m}^2$, $C_{2KF} = -3.80 \mu\text{m}^4$; $C_{0Y} = -0.12$, $C_{1Y} = -14.87 \mu\text{m}^2$, $C_{2Y} = 39.01 \mu\text{m}^2$, $C_{3Y} = -6.43 \mu\text{m}^4$.

$$A_{KF} = \frac{\pi}{\sqrt{C_{1KF} - C_{0KF}}} \int_{\chi_l}^{\chi_u} \sqrt{\frac{(C_{1KF} + C_{0KF})\chi^2 - 2(C_{1KF}^2 - 4C_{2KF})\chi + (C_{1KF} - C_{0KF})(C_{1KF}^2 - 4C_{2KF})}{\chi^2 - 2(C_{1KF} - C_{0KF})\chi - 2C_{1KF}C_{0KF} + C_{1KF}^2 + 4C_{2KF}}} d\chi, \quad (15a)$$

where

$$\chi_l = \sqrt{C_{1KF}^2 - 4C_{2KF}} \quad \text{and} \quad \chi_u = \sqrt{C_{1KF}^2 - 4C_{2KF} + 2(C_{1KF} - C_{0KF}) \left(\sqrt{C_{0KF}^2 - 4C_{2KF} - C_{0KF}} \right)};$$

$$V_{KF} = \frac{\pi}{2(C_{1KF} - C_{0KF})^{3/2}} \int_{\chi_l}^{\chi_u} \chi \sqrt{-\chi^2 + 2(C_{1KF} - C_{0KF})\chi - (C_{1KF}^2 + 4C_{2KF} - 2C_{1KF}C_{0KF})} d\chi; \quad (15b)$$

$$\Psi_{KF} = \frac{\pi^{1/3}(6V_{KF})^{2/3}}{A_{KF}}. \quad (15c)$$

3.4. Yurkin’s model

Based on Eq. (13), Yurkin proposed the following four-parametric model (see p. 127 in [2]), describing the meridional cross-section of a RBC

$$x^4 + 2C_{0Y}x^2z^2 + z^4 + C_{1Y}x^2 + C_{2Y}z^2 + C_{3Y} = 0, \quad (16)$$

where the relationship between the parameters of the model C_{iY} , $i = 0, 1, 2, 3$ and the morphological ones is

$$C_{1Y} = -\frac{D^2}{4} - \frac{\tau_{\min}^2 \tau_{\max}^2}{4D^2} + \frac{\tau_{\min}^2 d^2}{4D^2(\tau_{\max}^2 - \tau_{\min}^2)}, \quad (17a)$$

$$C_{2Y} = \frac{D^4 + 4D^2C_{1Y} - \tau_{\min}^4}{4\tau_{\min}^2};$$

$$C_{3Y} = -\frac{D^2}{16}(D^2 + 4C_{1Y}), \quad (17b)$$

$$C_{0Y} = -\frac{d^2 + 2C_{1Y}}{\tau_{\max}^2}.$$

The surface area, volume and sphericity index corresponding to Yurkin’s model can be obtained by using Eq. (3), in which the function

$$z = \left\{ \left[(2C_{0Y}x^2 + C_{2Y})^2 - 4(x^4 + C_{1Y}x^2 + C_{3Y}) \right]^{1/2} - 2C_{0Y}x^2 - C_{2Y} \right\}^{1/2} \quad (18)$$

has to be substituted. The limits of integration are $[0; D/2] \equiv [0; 2^{-1/2} \sqrt{(C_{1Y}^2 - 4C_{3Y})^{1/2} - C_{1Y}}]$

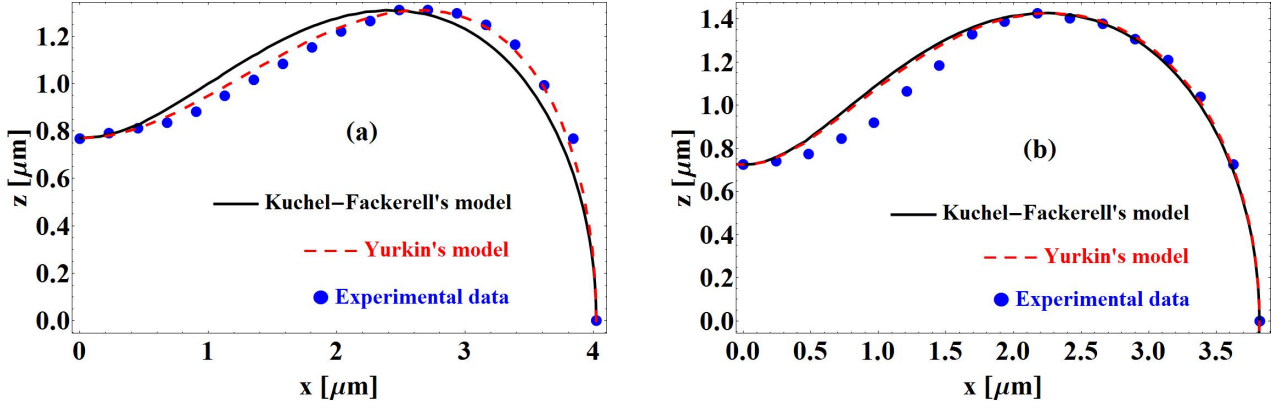


Fig. 6. Contours of RBCs modeled via Kuchel–Fackerell’s model (—) and Yurkin’s one (---) in comparison to experimentally obtained contours [Cell 3 in (a)] and [Cell 4 in (b)] (•) of normal red blood cells taken from [5]. For the parameters of the considered models in case (a) one has: $C_{0KF} = -15.11 \mu\text{m}^2$, $C_{1KF} = 28.04 \mu\text{m}^2$, $C_{2KF} = -16.98 \mu\text{m}^4$; $C_{0Y} = 0.17$, $C_{1Y} = -14.61 \mu\text{m}^2$, $C_{2Y} = 41.60 \mu\text{m}^2$, $C_{3Y} = -25.02 \mu\text{m}^4$, while in case (b) their values are as follows: $C_{0KF} = -14.08 \mu\text{m}^2$, $C_{1KF} = 15.06 \mu\text{m}^2$, $C_{2KF} = -8.19 \mu\text{m}^4$; $C_{0Y} = 0.9$, $C_{1Y} = -14.03 \mu\text{m}^2$, $C_{2Y} = 15.06 \mu\text{m}^2$, $C_{3Y} = -8.19 \mu\text{m}^4$.

4. POLYNOMIAL APPROXIMATIONS WITH A DEGREE HIGHER THAN FOUR

4.1. Fung-Tong’s model

The model proposed by Fung and Tong [27] is based on a three-parametric polynomial of the form

$$\left(\frac{2z}{D}\right)^2 = \left[1 - \left(\frac{2x}{D}\right)^2\right] \times \left[C_{0FT} + C_{1FT} \left(\frac{2x}{D}\right)^2 + C_{2FT} \left(\frac{2x}{D}\right)^4\right], \quad (19)$$

For the relationship between the parameters C_{iFT} , $i = 0, 1, 2$ and those characterising the geometry of the

cell one has

$$\begin{aligned} C_{0FT} &= \frac{\tau_{\min}^2}{D^2}, \\ C_{1FT} &= \frac{D^2}{d^2} \left[\frac{\tau_{\max}(2D^2 - 3d^2)}{(D^2 - d^2)^2} - 2C_{0FT} \right], \\ C_{2FT} &= \frac{D^4}{d^4} \left[C_{0FT} - \frac{\tau_{\max}^2(D^2 - 2d^2)}{(D^2 - d^2)^2} \right]. \end{aligned} \quad (20)$$

In integral form, for the surface area, volume and sphericity index within the framework of the model one finds

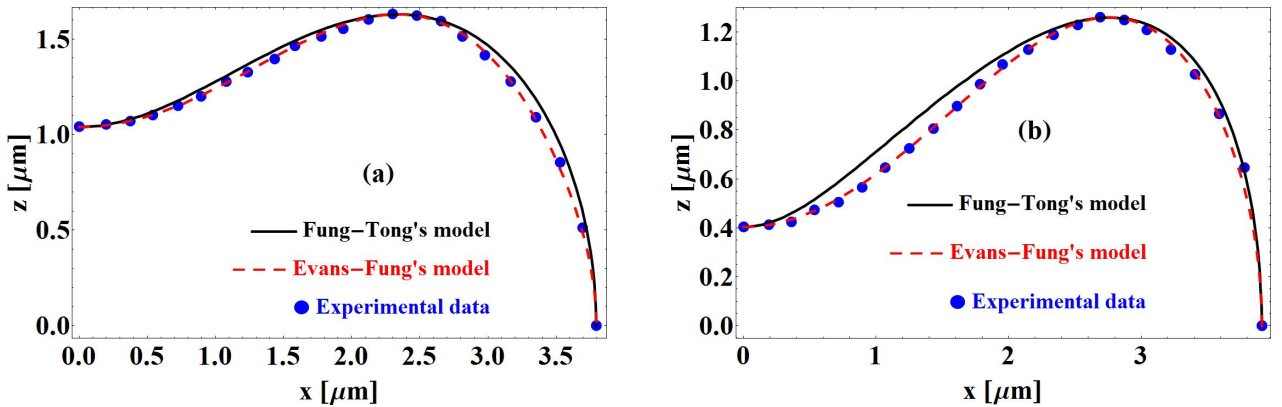


Fig. 7. Contours of RBCs modeled via Fung–Tong’s model (—) and the Evans-Fung’s one (---) in comparison to an experimentally obtained contours [Cell 1 in (a)] and [Cell 2 in (b)] (•) of normal red blood cells taken from [4]. For the parameters of the considered models in case (a) one has: $C_{0FT} = 0.075$, $C_{1FT} = 0.691$, $C_{2FT} = -0.277$; $C_{0EF} = 0.274$, $C_{1EF} = 0.988$, $C_{2EF} = -0.721$, while in case (b) their values are as follows: $C_{0FT} = 0.011$, $C_{1FT} = 0.375$, $C_{2FT} = 0.038$; $C_{0EF} = 0.104$, $C_{1EF} = 0.957$, $C_{2EF} = -0.505$.

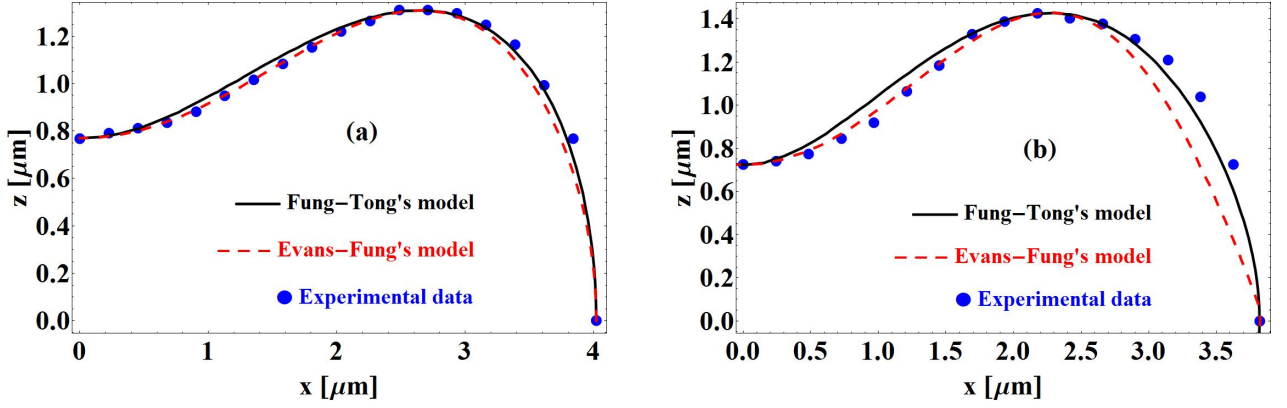


Fig. 8. Contours of RBCs modeled via Fung–Tong’s model (—) and the Evans–Fung’s one (---) in comparison to experimentally obtained contours [Cell 3 in (a)] and [Cell 4 in (b)] (•) of normal red blood cells taken from [5]. For the parameters of the considered models in case (a) one has: $C_{0FT} = 0.037$, $C_{1FT} = 0.363$, $C_{2FT} = -0.036$; $C_{0EF} = 0.192$, $C_{1EF} = 0.730$, $C_{2EF} = -0.399$, while in case (b) their values are as follows: $C_{0FT} = 0.036$, $C_{1FT} = 0.685$, $C_{2FT} = -0.491$; $C_{0EF} = 0.190$, $C_{1EF} = 1.197$, $C_{2EF} = -1.178$.

$$A_{FT} = \frac{\pi D^2}{2} \int_0^1 \sqrt{1 + \frac{(1-\chi)[(C_{0FT} + C_{1FT} + C_{2FT}) - 2(C_{1FT} + 2C_{2FT})\chi + 3C_{2FT}\chi^2]^2}{\chi[(C_{0FT} + C_{1FT} + C_{2FT}) - (C_{1FT} + 2C_{2FT})\chi + C_{2FT}\chi^2]}} d\chi; \quad (21a)$$

$$V_{FT} = \frac{\pi D^3}{4} \int_0^1 \sqrt{\chi[(C_{0FT} + C_{1FT} + C_{2FT}) - (C_{1FT} + 2C_{2FT})\chi + C_{2FT}\chi^2]} d\chi; \quad (21b)$$

$$\Psi_{FT} = \frac{\pi^{1/3}(6V_{FT})^{2/3}}{A_{FT}}. \quad (21c)$$

In Ref. [24], the authors credited this model to Skalak [28], although it was first introduced by Fung and Tong (compare Eq. (24) from [27] with the one given in Figure 7 (a) in [28]).

4.2. Evans–Fung’s model

In order to approximate the obtained experimental results for the thickness distribution of RBCs, Evans and Fung proposed the following three-parametric model [4]

$$\left(\frac{2z}{D}\right)^2 = \left[1 - \left(\frac{2x}{D}\right)^2\right] \times \left[C_{0EF} + C_{1EF}\left(\frac{2x}{D}\right)^2 + C_{2EF}\left(\frac{2x}{D}\right)^4\right]^2, \quad (22)$$

where one finds for the relationship between the model parameters and the morphological ones the following expressions

$$\begin{aligned} C_{0EF} &= \frac{\tau_{\min}}{D}, \\ C_{1EF} &= \frac{D^2}{2d^2} \left[-4C_{0EF} + \frac{\tau_{\max}|5d^2 - 4D^2|}{(D^2 - d^2)^{3/2}}\right], \\ C_{2EF} &= \frac{D^4}{2d^4} \left[2C_{0EF} + \frac{\tau_{\max}(2D^2 - 3d^2)}{\text{sgn}(5d^2 - 4D^2)(D^2 - d^2)^{3/2}}\right]. \end{aligned} \quad (23)$$

The corresponding expressions for the surface area, volume and sphericity index are

$$A_{EF} = \frac{\pi D^2}{2} \int_0^1 \sqrt{1 + \frac{(1-\chi)[(C_{0EF} + C_{1EF} + C_{2EF}) - 3(C_{1EF} + 2C_{2EF})\chi + 5C_{2EF}\chi^2]^2}{\chi[(C_{0EF} + C_{1EF} + C_{2EF}) - (C_{1EF} + 2C_{2EF})\chi + C_{2EF}\chi^2]}} d\chi; \quad (24a)$$

$$\begin{aligned} V_{EF} &= \frac{\pi D^3}{4} \int_0^1 \sqrt{\chi[(C_{0EF} + C_{1EF} + C_{2EF}) - (C_{1EF} + 2C_{2EF})\chi + C_{2EF}\chi^2]} d\chi \\ &= \pi D^3 \frac{(35C_{0EF} + 14C_{1EF} + 8C_{2EF})}{210}, \end{aligned} \quad (24b)$$

$$\Psi_{EF} = \frac{\pi^{1/3}(6V_{EF})^{2/3}}{A_{EF}}. \quad (24c)$$

Here we note, that the reader can find a slight modification of this model in Ref. [29], where the authors introduced an additional factor (the aspect ratio $\eta \equiv \tau_{\max}/D$) in the right hand side of Eq. (22).

5. DISCUSSION AND CONCLUDING REMARKS

In the current article we have summarized the existing polynomial approximations of the meridional cross-section of a RBC, and compared each model to a set of experimental data. For every model we have given the relationship between the parameters that characterise it and the ones describing the geometry of the biconcave shape (cross-section), namely D , d , τ_{\max} , and τ_{\min} .

We started with the lowest degree polynomial approximation – Beck’s model – representing second order polynomial [see Eq. (1)], where the obtained expressions for the relationship between the model parameters and the morphological ones [see Eq. (2)], as well as the expressions for the surface area and volume [see Eqs. (4a)] were derived by the author. The comparison with the experimental data is shown in Figures 1 and 2.

Following this model we have commented on four quartic polynomial models, first of which was the one based on Cassinian ovals [see Eq. (5) in Section 3.1]. Here we showed that the relationship between the parameters of the model and the morphological ones is not unique, which generates two distinct curves, resembling the RBC’s meridional cross section [see

Figures 3 and 4]. Here we derived explicit expressions for the surface area, volume and sphericity index, see Eqs. (8). An interesting observation about the model is that when $\varepsilon \rightarrow \infty$ (or equivalently $a \rightarrow 0$), $\mathcal{A}_C \rightarrow 1$, $\mathcal{V}_C \rightarrow 1$ and consequently $\Psi_C \rightarrow 1$. This justifies the obtained results, due to the fact that when $a \rightarrow 0$ the foci of the Cassinian ovals coincide with the zero of the coordinate frame and Eq. (5) describes the cross-section of a sphere with radius c , surface area $4\pi c^2$ and volume $(4/3)\pi c^3$. By definition the sphericity index of a spherical particle is unity.

After slightly modifying Eq. (5) by introducing an additional degree of freedom [see Eq. (9)], we obtained an unique relationship between the model and morphological parameters, as can be clearly seen from Figures 3 and 4, thus achieving a better approximation than that based on the standard Cassinian ovals equation. Within this model, expressions for A , V and Ψ were also obtained [see Eq. (12)].

The last two models of Section 3 are those of Kuchel-Fackerell [see Eq. (13)] and Yurkin [see Eq. (16)]. Unfortunately due to the complexity of these two models, the expressions for A , V and Ψ are only given in integral form. The given relations between the parameters were derived by the authors. Looking at Figures 5 and 6, one can conclude that the modification introduced by Yurkin is significant. Note that so far all model parameters were related to only three morphological ones – D , τ_{\max} , and τ_{\min} . The introduction of a fourth pa-

Table 2. Tabular comparison between the experimental values (first row) of the surface area (A [μm^2]), volume (V [μm^3]) and sphericity index (Ψ) of four different experimentally obtained mean red blood cell contours and different approximating models - Beck’s model (B), models based on single loop Cassinian (CO) and generalized Cassinian (gCO) ovals, Kuchel-Fackerell’s model (KF), Yurkin’s model (Y), Fung-Tong’s model (FT) and Evans-Fung’s model (EF).

Model	Cell 1			Cell 2			Cell 3			Cell 4		
	A	V	Ψ									
Exp. data	135	116	0.852	135	94	0.741	134	99	0.771	129	95	0.776
B	134	117	0.863	134	91	0.730	139	105	0.774	132	103	0.805
CO*	129	110	0.861	135	107	0.807	134	122	0.832	129	105	0.834
CO [†]	158	131	0.790	108	77	0.810	105	78	0.841	129	105	0.834
gCO**	134	119	0.873	130	96	0.780	135	107	0.807	129	105	0.834
KF	133	118	0.875	131	96	0.774	137	108	0.801	129	105	0.834
Y	137	122	0.868	135	97	0.756	140	110	0.793	130	105	0.828
FT	136	120	0.865	135	97	0.756	140	110	0.793	127	102	0.831
EF	133	116	0.865	134	93	0.741	138	107	0.780	123	93	0.807

*The parameters of the model are (a_1, c_1) [see Eq. (7a)]

[†]The parameters of the model are $(a_{3,+}, c_{3,+})$ [see Eq. (7c)]

**The parameters of the model are (a_g, b, c_g) [see Eq. (11)]

parameter allowed Yurkin to include in his model additionally the parameter d (the diameter of a circle that determines the location of the maximum thickness) [see Eq. (17)], and by that to improve the approximating ability of the polynomial suggested by Kuchel and Fackerell.

Last but not least we have considered the models by Fung and Tong [see Section 4.1] and Evans and Fung [see Section 4.2]. The first, described by a three-parametric sixth degree polynomial [see Eq. (19)] while the second – by a three-parametric eight degree one [see Eq. (22)]. Here we managed to obtain the relationship between the model and morphological parameters [see Eqs. (20) and (23)], as well as integral expressions for the surface area, volume and sphericity index. The comparison with the experimental data is depicted on Figures 7 and 8. The comparison between the experimental and model calculated quantities A , V and Ψ is shown in Table 2.

REFERENCES

- [1] L. Bi, and P. Yang, *J. Biomed. Opt.* **18**, 055001 (2013).
- [2] M. Yurkin, *Discrete dipole simulations of light scattering by blood cells*, Ph.D. thesis, University of Amsterdam (2007).
- [3] J. S. Beck, *J. Theor. Biol.* **75**, 587–501 (1978).
- [4] E. Evans, and Y.-C. Fung, *Microvasc. Res.* **4**, 335–347 (1972).
- [5] A. Jay, *Biophysical Journal* **15**, 205–222 (1975).
- [6] J. Steward, *Calculus*, Cengage Learning, 2012, 7th edn.
- [7] H. J. Deuling, and W. Helfrich, *Biophys J.* **16**, 861–868 (1976).
- [8] H. Funaki, *Jpn. J. Physiol.* **5**, 81–92 (1955).
- [9] P. Canham, *Journal of Theoretical Biology* **26**, 61–81 (1970).
- [10] H. W. Vayo, *Can. J. Physiol. Pharmacol.* **61**, 646–649 (1983).
- [11] H. W. Vayo, and M. K. Shibata, *Jap. J. Physiol.* **34**, 357–360 (1984).
- [12] Y. Fan, and W. Wang-yi, *Appl. Math. Mech. (English Edition)* **8**, 17–30 (1987).
- [13] L. D. Spears, *Theoretical constructs and the shape of the human erythrocyte*, Ph.D. thesis, Southern Illinois University at Carbondale (1993).
- [14] V. Kralj-Iglic, S. Svetina, and B. Zeks, *Eur. Biophys. J.* **22**, 97–103 (1993).
- [15] P. Mazon, and S. Müller, *J. Opt.* **29**, 68–77 (1998).
- [16] B. Angelov, and I. Mladenov, “On the Geometry of Red Blood Cell,” in *Geometry, Integrability and Quantization*, edited by I. Mladenov, and G. Naber, Coral Press, 2000, vol. 1, pp. 27–46.
- [17] I. M. Mladenov, *Comptes Rendus de l’Academie Bulgare des Sciences* **53**, 13–16 (2000).
- [18] C. A. Long, “Mathematical models and enigmas in evolution of erythrocytes,” in *Proceedings of the 2006 WSEAS International Conference on Mathematical Biology and Ecology, Miami, Florida, USA, January 18-20, 2006*, pp. 74–80.
- [19] A. Di Biasio, and C. Cametti, *Bioelectrochemistry* **71**, 149–156 (2007).
- [20] J. O. Ricardo, M. Muramatsu, F. Palacios, M. Gesualdi, O. Font, J. L. Valin, M. Escobedo, S. Herold, D. F. Palacios, G. F. Palacios, and A. Sánchez, *J. Phys. Conf. Ser.* **274**, 012066 (2011).
- [21] K. A. Melzak, G. R. Lázaro, A. Hernández-Machado, I. Pagonabarraga, J. de Espadae, and J. L. Toca-Herrera, *Soft Matter* **8**, 7716–7726 (2012).
- [22] J. Hellmers, E. Eremina, and T. Wriedt, *J. Opt. A: Pure Appl. Opt.* **8**, 1–9 (2006).
- [23] E. Eremina, H. J. Y. Eremin, and T. Wriedt, *Journal of Quantitative Spectroscopy & Radiative Transfer* **102**, 3–10 (2006).
- [24] T. Wriedt, J. Hellmers, E. Eremina, and R. Schuh, *Journal of Quantitative Spectroscopy and Radiative Transfer* **100**, 444–456 (2006).
- [25] D. Dantchev, and G. Valchev, *Journal of Colloid and Interface Science* **372**, 148–163 (2012).
- [26] P. W. Kuchel, and E. D. Fackerell, *Bull. Math. Biol.* **61**, 209–220 (1999).
- [27] Y. B. Fung, and P. Tong, *Biophysical Journal* **8**, 175–198 (1968).
- [28] R. Skalak, A. Tozeren, R. P. Zarda, and S. Chien, *Biophys J.* **3**, 245–264 (1973).
- [29] M. A. Yurkin, K. A. Semyanov, P. A. Tarasov, A. V. Chernyshev, A. G. Hoekstra, and V. P. Maltsev, *Appl. Opt.* **44**, 5249–5256 (2005).

ВЪРХУ РАЗЛИЧНИТЕ МОДЕЛИ, ОПИСВАЩИ РАВНОВЕСНАТА ФОРМА НА ЕРИТРОЦИТ

Г. Вълчев, В. Василев, П. Джонджоров

Институт по механика, Българска академия на науките, ул. "Акад. Г. Бончев", блок 4, 1113 София, България

(Резюме)

Като един от най-важните типове кръвни клетки във всички гръбначни организми, изучаването на равновесната форма на еритроцитите е от особена важност за разбирането на техните физико-химични и механични свойства. Настоящата работа представлява обобщение на съществуващите до момента модели и методи, описващи равновесната форма на червените кръвни клетки. Започвайки с най-опростения модел – този базиран на овали на Касини и завършвайки с най-общия вид на уравнението за формата на ососиметрични флуидни мембрани, ние правим сравнение на всеки от моделите с набор от експериментални данни. Целта ни е да създадем класификация на моделите за специфичните цели на тяхното приложение, като например за аналитично изучаване на взаимодействията между отделните еритроцити или между тях и стените на кръвоносните съдове, за диагностика на заболявания, свързани с промяна на равновесната форма на клетките, както и за експериментално изучаване на червените кръвни телца чрез разсейване на светлина.